Fluid Helium in a Narrow Pore at Zero Temperature

Journal of Low Temperature Physics

ISSN 0022-2291
Volume 162
Combined 5-6

J Low Temp Phys (2010)
162:583-589
DOI 10.1007/
s10909-010-0238-8

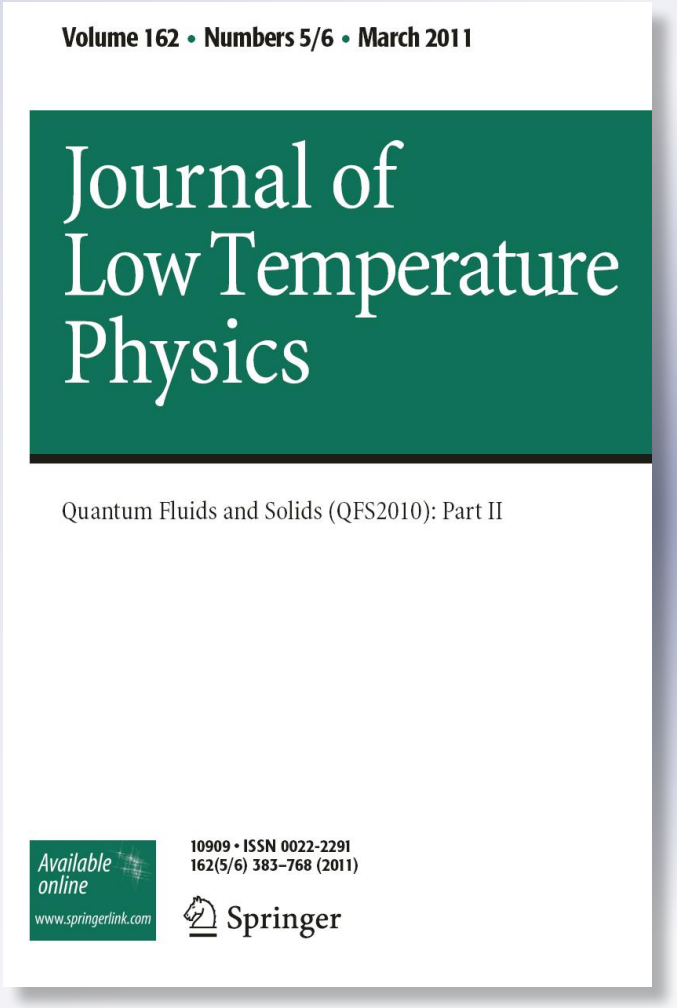

Springer

J Low Temp Phys (2011) 162: 583–589
DOI 10.1007/s10909-010-0238-8

Fluid Helium in a Narrow Pore at Zero Temperature

E.S. Hernández

Received: 11 June 2010 / Accepted: 29 September 2010 / Published online: 19 October 2010

Abstract The zero temperature adsorption isotherm of ^{4}He in a rigid cylindrical pore with alkali metal walls is computed within finite-range density functional theory, with the radius of the tube as a parameter. It is shown that starting from narrow pores and increasing the radius, the adsorbed helium first becomes bound in a quasi-onedimensional phase, and finally condenses into a quasi-twodimensional configuration by going through an almost filling situation. The results are in agreement with recent calculations for carbon nanotubes based on thermodynamical approaches.

Keywords Helium adsorption · Variable radius · Quasitransition

1 Introduction

Recently, condensation of fluids in cylindrical pores of varying radii attracted attention [1–3]. The response of the walls of carbon nanotubes to the pressure exerted by the adsorbed material can be mimicked within a simple but sound thermodynamic description, that permits to examine the adsorption isotherms of a gas within a swelling or shrinking pore, with physical input such as the equation of state (EOS) of a quasi-onedimensional (Q1D) gas, of the fluid–substrate interaction, and of the elastic energy of the tube, and it has been shown that a transition from a Q1D to a quasi-twodimensional (Q2D) fluid can take place along a given isotherm. It is worth recalling here that a system is Q1D when the energy requested to excite the radial

E.S. Hernández (✉)
Departamento de Física, Facultad de Ciencias Exactas y Naturales, Universidad de Buenos Aires, 1428 Buenos Aires, Argentina
e-mail: shernand@df.uba.ar

E.S. Hernández
Consejo Nacional de Investigaciones Científicas y Técnicas, Buenos Aires, Argentina

motion of the atoms—*i.e.*, perpendicular to the axis of the tube, say z—is much higher than the energy associated to displacements along the z-axis. A similar definition holds for the Q2D case. In this work I illustrate the adsorption path of helium at zero temperature for different radii and show that this type of transition can be expected regardless the adsorbing power. As shown in previous work, finite-range density functional (FRDF) calculations permit to establish the EOS of helium atoms under different confinements (see, *e*.g., Refs. [4, 5] and refs. therein). The general method is applied to the investigation of condensation of helium in a cylindrical pore of radius R and length L, with the same density functional employed in Refs. [6–8], whose detailed description and parameters can be found in Ref. [12]. In particular, Cs substrates of diverse shapes are excellent candidates to investigate nontrivial aspects of the physics of wetting, since the soft He-Cs potential, that prevents helium from condensing into a thick film on planar Cs surfaces at zero temperature, can be substantially enhanced by curving or folding the plane, giving rise, for example, to filling of linear wedges of intermediate openings [9], of infinite pores with polygonal section [10] as well as cavities on a nanostructured surface [5, 11]. One additional advantage of carrying FRDF calculations with alkali metal surfaces is the substantial reduction in computing time with respect to the very strong graphite substrate, yielding results which are qualitative akin to those expected for very large adsorption strengths.

2 Single Helium Atom in a Cylindrical Pore

Prior to determining the EOS of helium in pores, for future reference I consider the binding of a single helium atom to an cylindrical sheet. The confining potential $V(r; R)$ was derived in Ref. [13] considering that one helium atom at radial distance r from the axis of the cylinder of radius R, interacts pairwise with atoms in the sheet of uniform areal density θ via a Lennard-Jones (LJ) potential of strength ε and core radius σ. The overall field at point r reads,

$$V(r; R) = 3\pi\varepsilon\sigma^2\theta\left[\frac{21}{32}\left(\frac{\sigma}{R}\right)^{10} M_{11}(r/R) - \left(\frac{\sigma}{R}\right)^{4} M_5(r/R)\right] \tag{1}$$

Here M_{2n+1} is an elliptic integral over angle φ (see Ref. [13]). For Cs walls the LJ parameters are $\varepsilon = 2.795$ K and $\sigma = 5.31$ Å; the adsorbing strength shows a very important reduction with respect to the graphite case, with corresponding values 16.87 K and 2.963 Å [6]. In fact, such a Cs nanotube is a theoretical artifact that renders the calculations possible, keeping the major structural trends unaffected, as shown in this work.

Illustrative results are shown in Figs. 1 and 2. Figure 1 displays, as functions of cylinder radius R, the potential $V(0, R)$ on the cylinder axis, the potential V_{min} at the absolute minimum, and the ground state (gs) energy ε_{gs} of one ^{4}He atom obtained by solving the single-particle (sp) Schrödinger equation in the cylindrical field[13]. The bulk chemical potential $\mu_0 = -7.15$ K is displayed as a reference, as well as the minimum potential $V_{min}(planar) = -11.3$ K of a planar Cs sheet and corresponding gs energy $\varepsilon(planar) = -5.83$ K. We note that the absolute minimum departs from

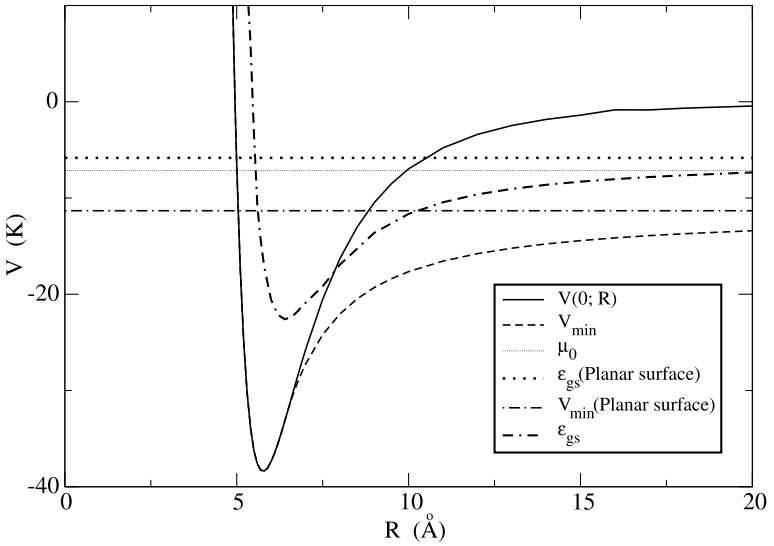

Fig. 1 Cylindrical potential $V(0; R)$ on the axis, potential V_{min} at the absolute minimum, and gs energy ε_{gs} of one ^{4}He atom, as functions of the cylinder radius R. The bulk chemical potential μ_0, the minimum potential of a planar Cs sheet and corresponding gs energy are also displayed. All energies are given in K

the axis at a radius of about 6.8 Å. On the other hand, the sp energy drops below the potential on the axis around $R = 7.5$ Å, signaling a threshold for the displacement of the probability density off-axis. This is further justified in Fig. 2, where the upper panel displays the potentials computed as in Ref. [13] due to Cs cylinders of different radius R, as functions of the radial distance r, and the lower panel shows the probability density of the He atom for the same radii.

From this figure we can learn an interesting pattern regarding adhesion of a single ^{4}He atom to a weakly binding surface rolled into a cylindrical wall. For the smallest radii here displayed, 5 and 6 Å, the probability density is concentrated on the axis, and on the wall for the largest radii 9 and 10 Å. In the intermediate regime, although the atom seeks the proximity of the wall, maximizing the wave function at the well minimum, still keeps a nonvanishing probability at $r = 0$, sizable for i.e., $R = 7$ Å. Note that the helium atom is unbound in a 5 Å tube; in fact, according to Fig. 1, the gs energy is negative for radii larger than 5.2 Å. Thus, a noninteracting Bose gas can be bound inside such pores into a Q1D axial phase, a filling regime and a Q2D shell phase, as the radius increases. For even larger radii, the usual layering structure of helium in a cavity [8] takes place.

3 Condensation of Helium in Cylindrical Pores

Applications of density functional theory reside in the construction of a specific energy density $\mathcal{E}[\rho(\mathbf{r})]$, where $\rho(\mathbf{r})$ is the particle density, normalized to the total number of helium atoms N so that, in the pore geometry, the linear density $n = N/(2\pi L)$

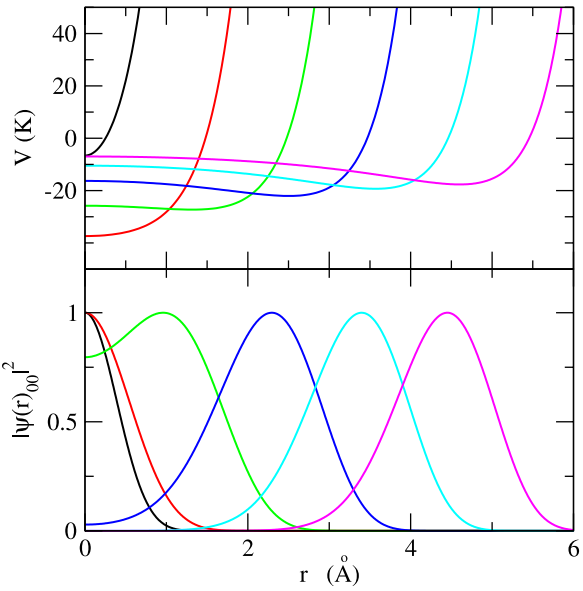

Fig. 2 (Color online) *Upper panel*: potentials of Cs cylinders (in K) parameterized by the radius for R between 5 and 10 Å, in steps of 1 Å from left to right. *Lower panel*: probability density of one ^{4}He atom in its ground state. The prodability distributions have been scaled to their respective maxima to facilitate comparison

is

$$n = \int dr r \rho(r) \tag{2}$$

The total energy $e = E/(2\pi L)$ of the ^{4}He atoms per unit length is then

$$e = \int dr r \mathcal{E}[\rho(r)] \tag{3}$$

The integrodifferential Euler-Lagrange equation is obtained by functional differentiation of (3) with respect to $\rho(r)$, and takes the form

$$\left[-\frac{\hbar^2}{2m}\left(\frac{d^2}{dr^2}+\frac{1}{r}\frac{d}{dr}\right)+U(\rho)+V(r;R)\right]\sqrt{\rho(r)} = \mu\sqrt{\rho(r)} \tag{4}$$

with μ the chemical potential of the helium atoms, $U(\rho) \equiv \delta\mathcal{E}/\delta\rho(r)$ the density-dependent mean field and $V(r, R)$ the adsorbing potential of a concave cylindrical sheet. As shown in previous work (see, *e.g.*, Ref. [12] and references therein), the chemical potential coincides with the energy per particle e/n for $N = 1$ (single atom binding) and in the thermodynamic limit, $N \longrightarrow \infty$.

Next, (4) is solved numerically in order to obtain the chemical potential, together with the total energy and the corresponding density profiles $\rho(r)$, as functions of the linear density n. Significant results are illustrated in Fig. 3, that shows the chemical potential and energy per particle for two selected pore radii, namely 6 and 9 Å, in full and dashed lines, respectively. For the narrowest pore, a stable Q1D system with negative grandpotential per unit length, $\omega = e - \mu$, is found for any linear density below 0.042 Å^{-1}, above which the system becomes unstable. For a sufficiently wide pore, the particle distribution has moved towards the cylinder wall and the EOS displays

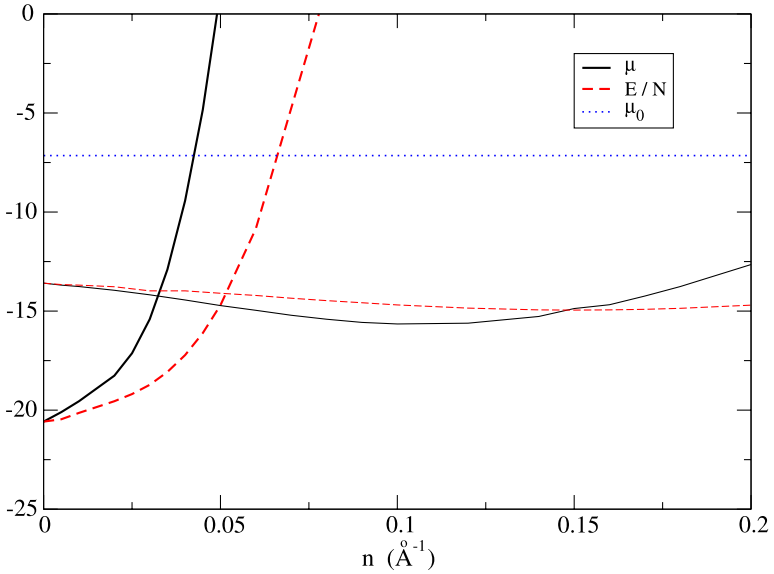

Fig. 3 (Color online) Chemical potential and energy per particle (in K) for ^{4}He atoms in Cs pores of radii $R = 6$ and 9 Å (*thick* and *thin lines*, respectively) as functions of linear density. The bulk chemical potential μ_0 is shown as a *dotted line*

the typical 2D prewetting jump at $n_{pw} = 0.15$ Å^{-1}, where the energy per particle becomes identical to the chemical potential of the sample, leading to condensation of a stable film at higher linear densities. This behaviour can be assessed by examining density profiles of ^{4}He atoms for various values of R at a given linear density, as displayed in Fig. 4 for $n = 0.05$ Å^{-1}. In this figure, the upper panel shows the total one-body field $U[\rho(r)] + V(r; R)$ experienced by particles in the fluid, together with the confining potential $V(r; R)$ (in dashed lines). The particle densities are plotted in the lower panel as functions of distance r. At first sight, in Fig. 4 we appreciate the persistence of the three regimes encountered in the sp pattern displayed in Fig. 2. Moreover, this plot provides evidence of the role of cohesion among ^{4}He particles and its competition with adhesion of atoms to the confining walls. The difference between full and dashed lines is the total interaction energy (per particle) of the interacting fluid and, as shown in various prior works [4, 6–8, 12] and references therein, consists of a screened LJ interaction plus two density-dependent correlation terms, one attractive, the other repulsive, in charge of representing in a phenomenological fashion, the effects of the many-body environment on the one-body field. For the two smallest radii, the overall outcome, as seen in the upper panel of Fig. 4, is a visible loss in potential energy and a distorsion of the potential well that causes an earlier departure of the minimum off-axis, as compared with the sp picture in Fig. 2. The situation is reversed for the largest radii. For $R = 9$ Å, the potential energy gain of about 2 K near the cylinder axis is sufficient to sustain a nonnegligible amount of fluid in that region. As a consequence, pores of radii between less than 7 and more than 9 Å can hold particle density distributed from axis to wall, and the appearance of the pure axial regime shifts towards larger radii. For radii near 12 Å and above,

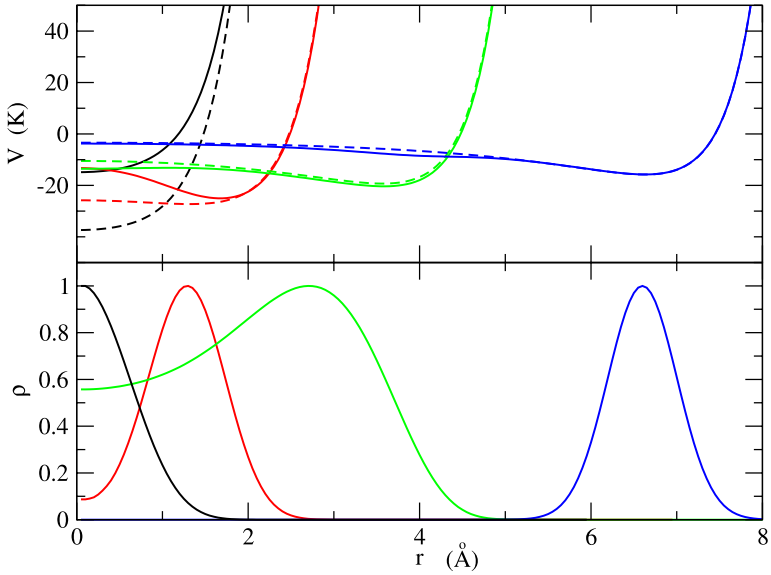

Fig. 4 (Color online) *Upper panel*: total mean-field potential in (4) (*full lines*) and potentials of a Cs cylinder as in Fig. 2 (*dashed lines*) for radii $R = 6, 7, 9$ and 12 Å from left to right. *Lower panel*: particle density for ^{4}He atoms at a linear density $n = 0.05$ Å^{-1}. The density distributions have been scaled to their respective maxima to facilitate comparison

the correlation effects in the helium fluid are negligible and the system behaves as a confined gas.

The density configurations may be compared with those for a carbon nanotube [14]. While for the much stronger adsorber one can see the coexistence of at least two peaks, respectively at the center and next to the pore wall, the much softer attraction of the alkali metal, together with the larger radial extension of the attractive well, permits a more important spread of the density near the axis for the smaller radii, and near the wall for $R = 12$ Å.

4 Summary

In this work, FRDF calculations of the equilibrium configuration of ^{4}He in a weakly adsorbing cylindrical pore show that, as the radius of the tube increases, a Q1D to Q2D transition takes place mediated by a filling regime. This is in agreement with theoretical findings based on thermodynamical approaches [1–3], although in the present model, the pore is rigid for each radius R, since data for the elastic energy of the material—that would permit a selfconsistent calculation of helium adsorption together with the response of the walls—are not available. Similar calculations for a carbon nanotube demand exceedingly large computing time at no extra benefit, since the present description already encompasses the main features of the adsorption and condensation scenario. Details of the interaction may give rise to layering effects

inside relatively small tubes, such as coexistence between axial and shell phases reported in previous work [14], which are absent for the much softer substrate presented here.

Acknowledgements This paper was prepared under support from grant X099 from University of Buenos Aires, Argentina. It is a pleasure to acknowledge hospitality at Penn State University where part of these calculations have been carried, and Milton Cole for interesting discussions.

References

1. H.-Y. Kim, S.M. Gatica, G. Stan, M.W. Cole, J. Low Temp. Phys. **156**, 1 (2009)
2. G. Stan, J. Low Temp. Phys. **157**, 374 (2009)
3. S.M. Gatica, H.-Y. Kim, J. Low Temp. Phys. **157**, 382 (2009)
4. M. Barranco, R. Guardiola, S. Hernández, R. Mayol, J. Navarro, M. Pi, J. Low Temp. Phys. **142**, 1 (2006)
5. F. Ancilotto, M. Barranco, E.S. Hernández, M. Pi, J. Low Temp. Phys. **157**, 174 (2009)
6. E.S. Hernández, M.W. Cole, M. Boninsegni, Phys. Rev. B **68**, 1254181 (2003)
7. E.S. Hernández, M.W. Cole, M. Boninsegni, J. Low Temp. Phys. **134**, 309 (2004)
8. E.S. Hernández, J. Low Temp. Phys. **137**, 89 (2004)
9. E.S. Hernández, F. Ancilotto, M. Barranco, R. Mayol, M. Pi, Phys. Rev. B **73**, 245406 (2006)
10. A. Hernando, E.S. Hernández, R. Mayol, M. Pi, Phys. Rev. B **77**, 195431 (2008)
11. F. Ancilotto, M. Barranco, E.S. Hernández, A. Hernando, M. Pi, Phys. Rev. B **79**, 1045141 (2009)
12. M. Barranco, M. Guilleumas, E.S. Hernández, R. Mayol, M. Pi, L. Szybisz, Phys. Rev. B **68**, 024515 (2003)
13. G. Stan, M.W. Cole, Surf. Sci. **395**, 280 (1998)
14. S.M. Gatica, G. Stan, M.M. Calbi, J.K. Johnson, M.W. Cole, J. Low Temp. Phys. **120**, 337 (2000)